Clinical Anatomy 8:1–16 (1995)

ORIGINAL COMUNICATIONS

Compromising Abnormalities of the Brachial Plexus as Displayed by Magnetic Resonance Imaging

JAMES D. COLLINS, MARLA L. SHAVER, ANTHONY C. DISHER, AND THEODORE Q. MILLER

UCLA School of Medicine, Department of Radiological Sciences (J.D.C.) and the Charles R. Drew Postgraduate School of Medicine, Department of Radiology (M.L.S., A.C.D., T.Q.M.), Los Angeles, California

Magnetic resonance images (MRI) of brachial plexus anatomy bilaterally, not possible by plain radiographs or CT, were presented to the Vascular Surgery, Neurology, and the Neurosurgery departments. Patients were requested for MRI of their brachial plexus. They were referred for imaging and the imaging results were presented to the faculty and housestaff. Our technique was accepted and adopted to begin referrals for MRI evaluation of brachial plexopathy. Over 175 patients have been studied. Eighty-five patients were imaged with the 1.5 Tesla magnet (Signa; General Electric Medical Systems, Milwaukee, WI) 3-D reconstruction MRI. Coronal, transverse (axial), oblique transverse, and sagittal plane T1-weighted and selected T2-weighted pulse sequences were obtained at 4–5 mm slice thickness, 40–45 full field of view, and a 512 × 256 size matrix. Saline water bags were used to enhance the signal between the neck and the thorax. Sites of brachial plexus compromise were demonstrated. Our technique with 3-D reconstruction increased the definition of brachial plexus pathology. The increased anatomical definition enabled the vascular surgeons and neurosurgeons to improve patient care. Brachial plexus *in vivo* anatomy as displayed by MRI, magnetic resonance angiography (MRA), and 3-D reconstruction offered an opportunity to augment the teaching of clinical anatomy to medical students and health professionals. Selected case presentations (body-builder, anomalous muscle, fractured clavicle, thyroid goiter, silicone breast implant rupture, and cervical rib) demonstrated compromise of the brachial plexus displayed by MRI. The MRI and 3-D reconstruction techniques, demonstrating the bilateral landmark anatomy, increased the definition of the clinical anatomy and resulted in greater knowledge of patient care management.

Key words: anatomy, brachial plexopathy, nerve model, neuropathy, MRI, pathology

INTRODUCTION

The anatomy of peripheral nerves and the brachial plexus is graphically displayed in classical textbooks (Clemente, 1985, 1987). Anatomical and clinico-pathologic nerve studies were published by Sunderland (1968) and pathologic alterations of peripheral nerve studies were studied by Dyck et al. (1984). The principles developed by these authors allow investigative radiological studies using multi-plane capabilities of magnetic resonance imaging (MRI) to step beyond textbook descriptions. MRI links the anatomy with the clinical pathology and allows better insight to peripheral nerve problems by displaying fascial plane structures according to proton density.

The brachial plexus lies within the fascial planes of the neck and axilla, but it is routinely displayed on MRI of the thorax and shoulder girdle (Collins et al., 1986). Magnetic resonance multiplane imaging allowed bilateral display of the thorax and brachial plexus in the

Received for publication March 22, 1994; revised September 6, 1994.

Address reprint requests to Dr. James D. Collins, UCLA School of Medicine, Department of Radiological Sciences, 10833 Le Conte Avenue, Los Angeles, CA 90024-1721.

supine position. This feature gave us an opportunity to image and study the brachial plexus when we described our first case report of autoimmune disease that resulted in compromising abnormalities of the brachial plexus (Collins et al., 1991a).

Abnormalities of the brachial plexus and/or brachial plexopathies result from problems with the cervico-thoracic levels of the vertebral column, the first rib, vascular supply, and soft tissues (Lord and Rosati, 1971; Lord, 1989). Surface and landmark anatomy is important for interpretation of MRI studies as is the neural patterns of the brachial plexus (Fig. 1). The anterior and middle scalene muscles, through which the brachial plexus nerve roots pass, arise from the cervico-thoracic levels of the vertebral column. The muscles insert and, in part, support the first rib. The first ribs are curved and flat and they slope obliquely to form most of the thoracic inlet. The slope which gives an anterior-superior directed upper surface, changes with respiration and effects structures crossing the rib. The scalene triangle is formed by the anterior scalene muscle and the posterior insertion of middle scalene muscle and the first rib. The upper nerve roots of the brachial plexus descend along the margin of the middle scalene muscle and join the lower nerve roots to envelope the subclavian artery. The nerve roots bind to the artery as shown in Figure 2a,b within the scalene triangle to form a neurovascular bundle (Lord and Rosati, 1971). This bundle passes with sympathetic fibers unprotected over the first rib through the scalene triangle, beneath the clavicle and subclavius muscle, inferior to the coracoid process, and posterior to the tendon of the pectoralis minor muscle into the axilla.

The subclavian artery, similar to the artery within the femoral triangle, is unprotected (Lord and Rosati, 1971; Clemente, 1987), but it is not routinely cannulated for vascular studies. Different from the femoral artery, a muscle (the anterior scalene) separates the subclavian vein from the subclavian artery. A thin layer of deep fascia envelopes the neurovascular supply of the upper limb and forms spaces from the root of the neck to the lower part of the axilla. The spaces which may have clinical problems that compromise the brachial plexus (Lord and Rosati, 1971) include the intervertebral foramina, scalene triangle, costoclavicular, costocoracoid, and the axilla. In most individuals, the

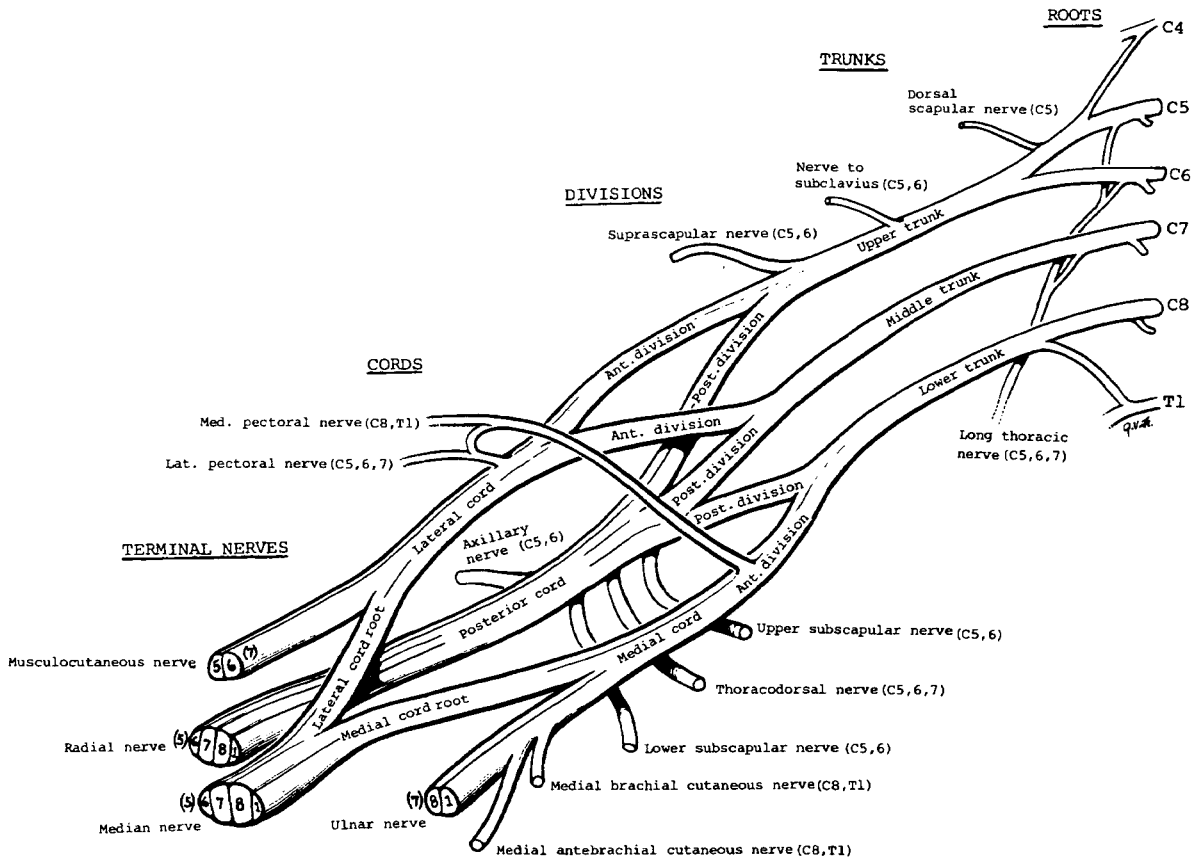

Fig. 1. Diagram of the brachial plexus. (from Clemente, C. D., Anatomy, An Atlas of the Human Body, 4th Ed., 1995, in press).

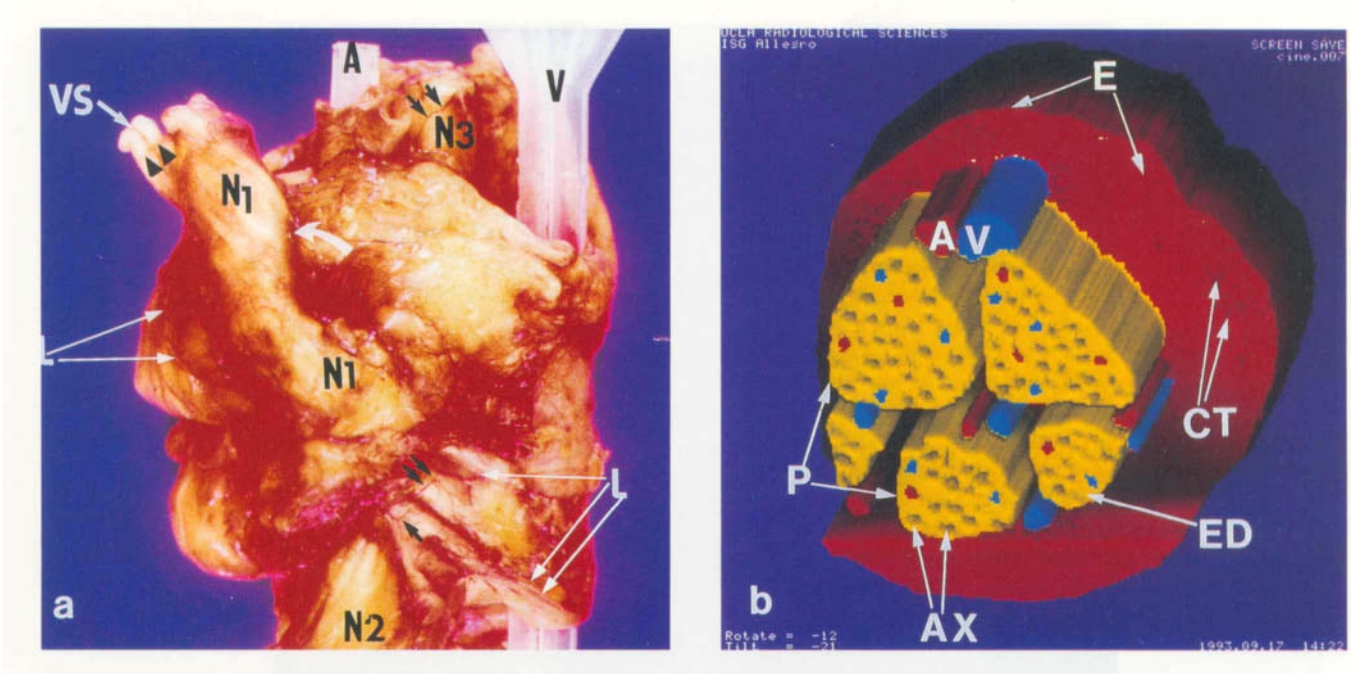

Fig. 2. **a**: This is the gross neurovascular specimen of the brachial plexus, artery and vein which was used to demonstrate nerves on MRI. The axillary nerve (black arrowheads) originates from the radial nerve (N1) which is bound (curved white arrow) to the axillary artery (A). The ulnar nerve is reflected inferiorly (N2) and the median nerve (N3) lies between the axillary artery (A) and vein (V). The nutrient arteries (black arrows) enter the nerves, a small plastic pipette is in the artery (A) and a larger pipette in the vein (V), lymphatics (L), vascular supply (VS). **b**: This is a 3-D computer generated transverse section of a peripheral nerve demonstrating the rich nutrient blood supply which Sunderland described in 1945. The collateral blood vessels have been omitted. Epineurium (EP), small dark capillaries (arrows) in the red connective tissue (CT), rich nutrient supply to nerves. Arteries (A), veins (V), perineurium (P), endoneurium (ED), axons (AX).

fascial plane spacing between soft tissues and osseous structures is adequate to perform routine functions without compromising their neurovascular bundles. Studies by Sunderland (1945) and Dyck et al. (1984) suggest pathology involving peripheral nerves alters fascial planes. The acute and/or permanent changes may alter the adjacent tissues, thereby compromising the vascular supply which nourishes the peripheral nerves. This results in patients presenting with clinical symptoms. They may also occur from articular motion of the shoulder girdle, hypertrophic enlargement of the scalene triangle muscles, congenital rib anomalies, pressure by ligaments, instances of abnormal insertion of the scalene muscles, fractures, primary and secondary tumors, crushing injuries of the thorax, and arteriosclerotic disease which results in thrombosis (Lord and Rosati, 1971; Sunderland, 1968). We also have reported autoimmune disease may result in similar compromise (Collins et al., 1991a). Degenerative changes of bone structures from aging and laxity of muscular structures results in complaints by patients of pre-existing compromising abnormalities that were not obvious problems at a younger age (Lord and Rosati, 1971).

MRI demonstrates soft-tissue detail by proton distribution and provides high resolution imaging of nerves, vascular structures, and the lymphatics (Collins et al., 1986, 1991b). The phospholipids that are found in the myelin of nerves are high intensity signals when visualized *in vitro* studies and intermediate to high intensity signals when demonstrated *in vivo*. Positive mode T1-weighted images show blood flow as low intensity signals (black) and subcutaneous fat as high intensity signals (white). This mode does not display the deep fascial layer of tissue containing the neurovascular compartments. The low intensity signals of blood and the high intensity signals of myelin combine to vary the signal intensity of nerves displayed on MRI dependent upon the selected level of imaging through the axis of the nerve (Collins et al., 1986). Nutrient vessels supply blood to peripheral nerves (Fig. 2a) and are visualized by MRI as low signal intensity vertical bands (Collins et al., 1989a; Sunderland, 1945). Since compression injuries of nerves involve an ischemic

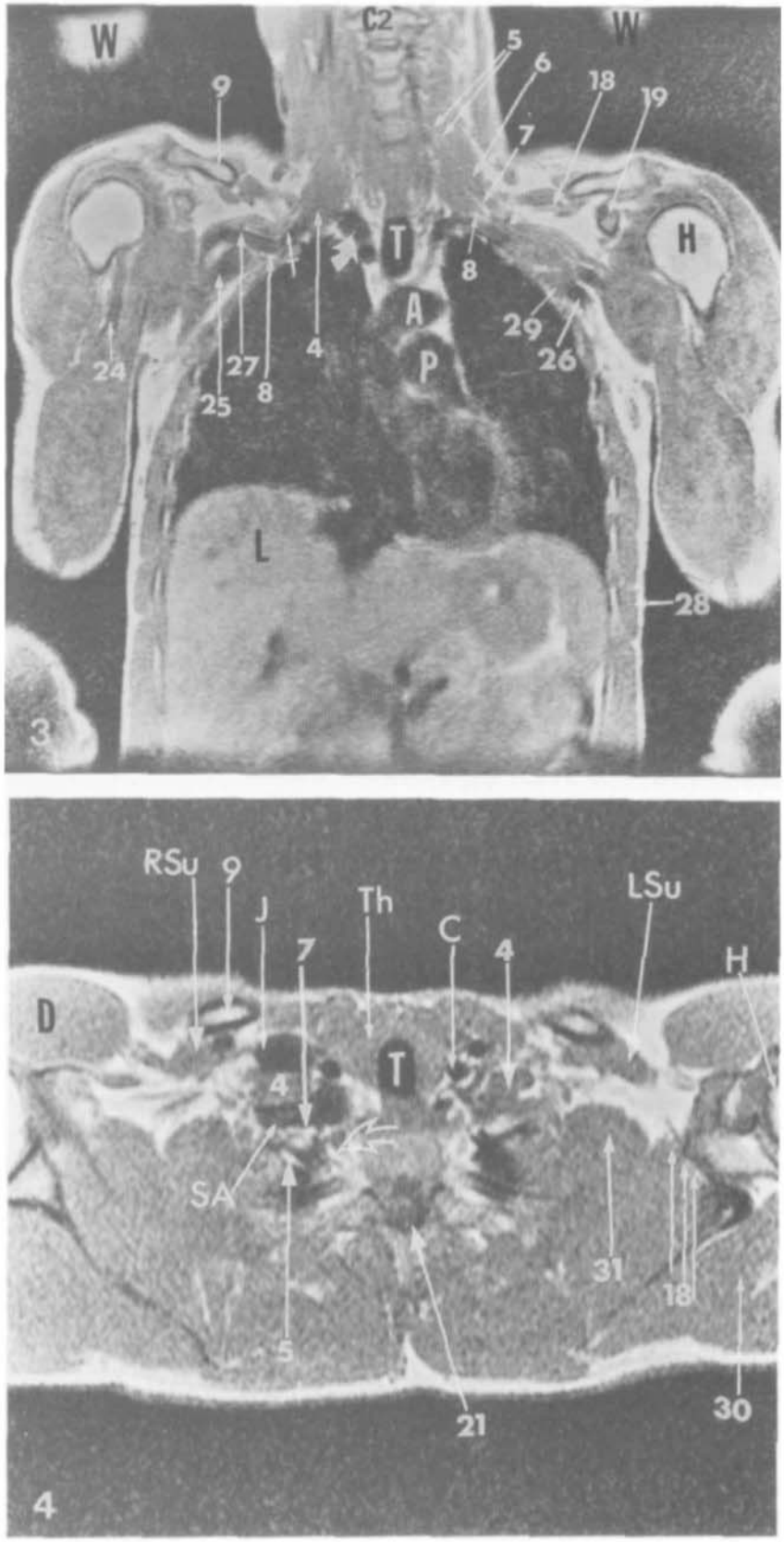
W
C2
W
5
6
18
19
9
7
T
H
8
A
29
26
4
27
24
P
25
8
L
28
3
RSu
9
J
Th
LSu
7
C
4
H
D
T
4
SA
31
18
5
21
30
4

Figs. 3 and 4

component, it seems impossible to compress a nerve without altering its blood supply (Sunderland, 1968). Ischemia initiates inflammatory changes causing edema and fibrosis. Inflammation and/or edema diminishes signal intensity of nerves and alters their architecture when compromised in autoimmune disease (Collins et al., 1991a).

Our group has developed a technique that allows bilateral imaging of the brachial plexus. This method is based upon the fact that the brachial plexus envelopes and adheres to a major artery forming a neurovascular bundle, and that displaying the artery insures imaging the nerves (Collins et al., 1986, 1989a). In 1985, we began to apply cursor lines (planes for the images) to the patient's chest in the coronal sequence in order to image the pleura for evaluating asbestos changes. The images obtained demonstrated detailed surface anatomy of the thoracic and shoulder girdle (Collins et al., 1986). Our anatomy department prepared a template list of anatomical structures to determine if our team could demonstrate the anatomy of the thorax and shoulder girdle with MRI. We imaged the prepared list, including bilateral imaging of the brachial plexus and used our results for teaching medical students, residents, and other health professionals (Collins et al., 1986, 1989b).

Following Sunderland's 1945 anatomic nerve model approach (Fig. 2b), Collins et al. (1989a) demonstrated with MRI the vascular low signal intensity that separates nerves from surrounding tissues. MRI of the brachial plexus is now an established technique. Immediate 3-D reformat reconstruction with 3-D color imaging enhances anatomy and pathology. Optical disks and videotape recordings make case material available for clinicians and enhance the teaching of radiology and pathology for larger audiences.

The purpose of this paper is to demonstrate landmark anatomy by MRI used for the detection of compromising brachial plexopathies. Bodybuilding, anomalous muscle, clavicle fracture, thyroid goiter, and silicone breast implant rupture are the cases selected for this communication (Collins et al., 1993). The MRI multiplane images of landmark anatomy and pathology are stressed here in order to improve patient care.

MATERIALS AND METHODS

Technique

Plain chest radiographs (PA and lateral) are obtained and reviewed prior to the MRI examination. The procedure is discussed and the patient examined. Respiratory gating is applied throughout the procedure to minimize motion artifact. The patient is supine in the body coil, arms down to the side and imaging is monitored at the MRI station.

A body coil is used because it offers optimal full field of view for bilateral imaging of the brachial plexus and provides uniform signal to noise ratio across the imaging field which is necessary for 3-D reconstruction. Surface coils are limited to depth and field of view and are not adequate for bilateral imaging of the brachial plexus. Intravenous contrast agents are not administered. A water bag (500 ml normal saline) is placed on the right and the left side of the neck above the shoulder girdle to increase signal to noise ratio for higher resolution imaging (Collins et al., 1993). A full field of view (40–48 cm) of the neck and the thorax is used to image both supraclavicular fossae. Contiguous (4–5 mm) coronal, transverse (axial), oblique transverse, and sagittal T1-weighted images are obtained. If there is clinical evidence of scarring, tumor and/or lymphatic obstruction, T2-weighted images are selectively ob-

Fig. 3. This is a coronal image through the scalene triangles demonstrating interscalene compression of the neurovascular bundles, right concave cervical spine scoliosis, and marked depression of vasculature, greater on the right than the left. The nerves have a high to intermediate signal intensity. Fascial plane fat (white) is virtually absent and measures only 4–5 mm in the subcutaneous tissues overlying the shoulder girdles. Second cervical vertebral body (C2), anterior scalene muscle (4), cervical nerve roots (5,6,7,8), clavicle (9), suprascapular nerve (18), coracoid process (19), tendon of the biceps muscle (24), dilated right axillary vein (25), left axillary vein (26), nutrient artery of the depressed middle trunk (27), fasicle of the serratus anterior muscle (28), pectoralis minor muscle (29), trachea (T), aorta (A), pulmonary artery (P), humerus (H), liver (L), saline water bags (W), beading of the right middle trunk nerve (single bar arrow).

Fig. 4. A transverse (axial) image at the level of the 7th cervical vertebral body demonstrating the large right anterior scalene muscle (4) compressing the low signal of the subclavian artery (RA) and the nerve roots. The larger first fasicle of the serratus anterior muscle (31) displaces the curved high signal intensity of the nerve trunks anteriorly against the left subclavius muscle (LSu). Trachea (T), thyroid (TH), jugular vein (J), left common carotid artery (C), humerus (H), right subclavius muscle (RSu), deltoid muscle (D), nerve roots (5, 7) and the 8th cervical nerve (curved clear arrow) crossing over the right lung, clavicle (9), suprascapular nerve (18) crossing the suprascapular notch, spinal cord tethered to the right (21), supraspinatus muscle (30).

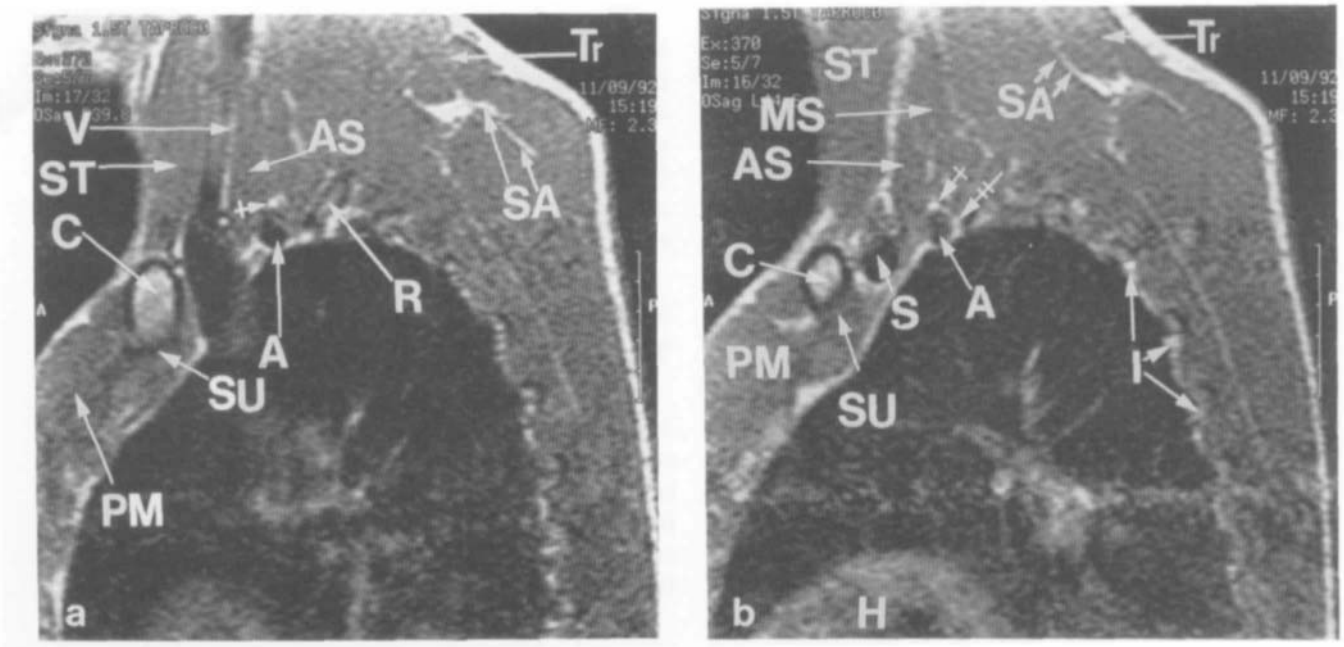

Fig. 5. **a**: This is an enlarged right sagittal image through the scalene triangle demonstrating the narrowed fascial plane between the anterior scalene muscle (AS) and the middle scalene muscle inserting on the first rib (R), inferior nerve trunk (bar arrow), clavicle (C), subclavian artery (A), subclavius tendon and muscle (SU), pectoralis major muscle (PM), sternocleidomastoid muscle (ST), vagus nerve (V), trapezius muscle (Tr), spinal accessory nerve (SA). **b**: This is an enlarged left sagittal image through the scalene triangle demonstrating the obscured fascial plane between the anterior scalene muscle (AS) and the middle scalene muscle (MS). Inferior nerve trunk (2-bar arrow), middle nerve trunk (bar arrow), clavicle (C), subclavian artery (A), subclavian vein (S), subclavius tendon and muscle (SU), pectoralis major muscle (PM), sternocleidomastoid muscle (ST), vagus nerve (V), trapezius muscle (Tr), spinal accessory nerve (SA), intercostal nerves (I), heart (H).

tained. Four imaging sequences are acquired, coronal, transverse, oblique transverse, and sagittal.

The coronal sequence is first to be imaged. The brachial plexus envelopes the artery (forming a neurovascular bundle) and the nerves are best imaged when the cursors are aligned to the arterial blood supply. The axillary artery margins vary in each patient and the cursors must be adjusted for each MRI brachial plexus examination. The cursors are positioned on the skin surface of the posterior chest wall to the skin surface of the anterior chest wall for symmetry, 3-D reconstruction, and to detect abnormalities that may mimic brachial plexopathies. The superior landmark is set at the base of the skull and the inferior landmark set at the level of the kidneys. The image that best demonstrates the arterial blood flow to the upper extremities is selected as the baseline image for the remaining sequences. The transverse sequence is set from the baseline coronal image at the superior aspect of the third cervical vertebral body to the carina. The lateral margins of the shoulder girdle are imaged to ensure bilateral, simultaneous display of the brachial plexus. The oblique transverse sequence is set by aligning the cursors to the arterial blood supply of each upper extremity using the baseline coronal sequence. The cursors are centered to the plane of the axillary artery 2 cm below the inferior cord of the brachial plexus to the superior margin of the coracoid process. This sequence is necessary to detect signal intensity, architecture, and effacement of the long axis of the nerves, arteries, and veins.

The sagittal sequence is obtained by aligning the cursors lateral to the coracoid process and medially to the insertion of the anterior scalene muscle on the first rib. The sagittal plane is necessary to detect effacement of the neurovascular bundle by the coracoid process, pectoralis minor muscle, clavicle and/or subclavius muscle, axillary masses, and abnormalities of the scalene triangle. When an image sequence is completed, it is immediately transferred to another screen at an independent workstation for review and 3-D reformat display. The software for this 3-D reconstruction is already prepared in the 1.5 Telsa G.E. Signa MRI unit. The images are stored on CT tape (GE 9800) format and on optical disks for 3-D color reconstruction on the ISG workstation. The entire study is monitored by the radiologist and requires 1.5 hours. Selected Kodak

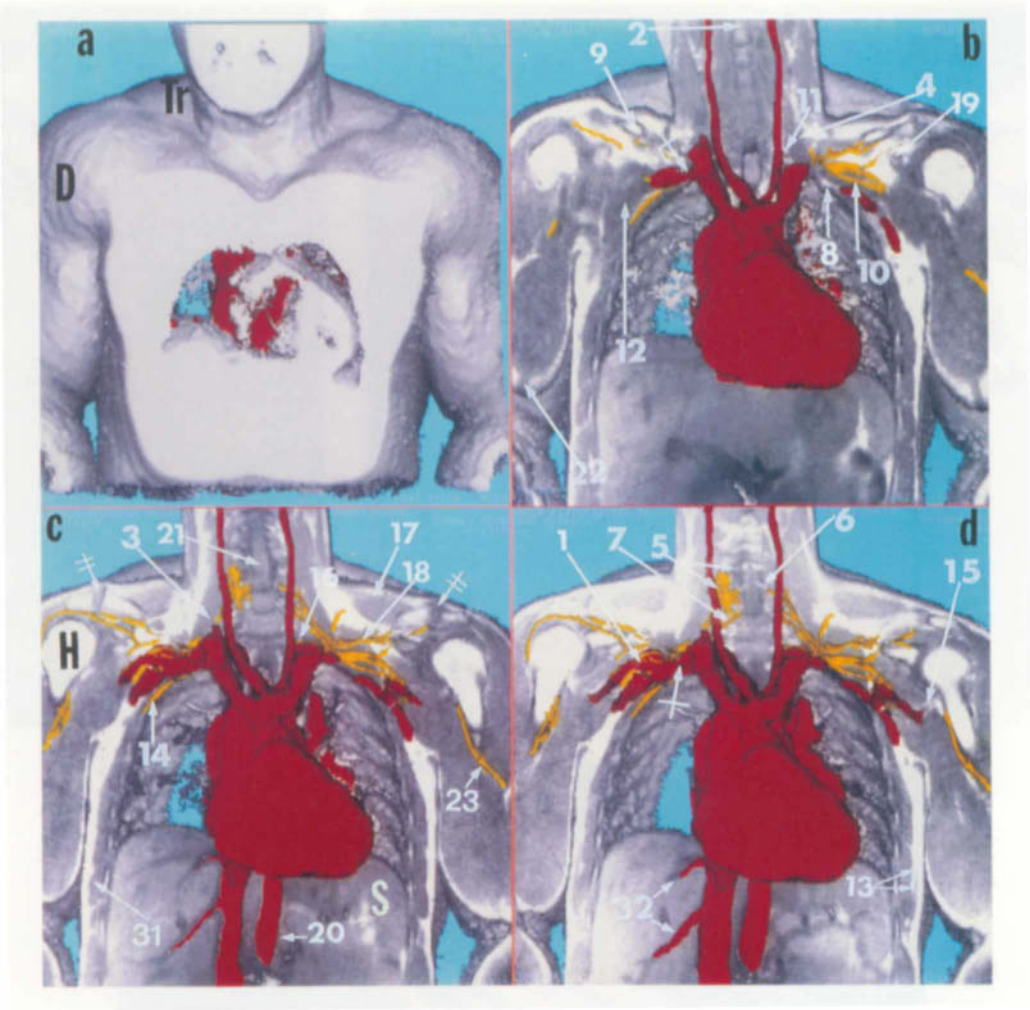

Fig. 6. This figure demonstrates a computer generated image (6a) and 3 serial coronal 3-D color reconstructed images. The shoulder girdle muscles are asymmetric (6a) and there are compressive changes of the right neurovascular bundle (bar arrows below 9 in 6b–d), compressed flattened arch of the left subclavian artery and vein (inferior to the first thoracic nerve) in Figure 6d. Post stenotic dilated axillary artery (1), second cervical vertebral body (2), anterior scalene muscle (3), middle scalene muscle (4), cervical nerve roots (5,6,7), inferior trunk (8), clavicle (9), middle trunk (10), phrenic nerve (11), pectoralis minor muscle (12), left long thoracic nerve (13), right long thoracic nerve (14), axillary nerve (15), supraspinatus muscle (17), suprascapular nerve (18), coracoid process (19), abdominal aorta (20), spinal cord (21), fasicle of serratus anterior muscle (31), basilic vein (22), musculocutaneus nerve (23), hepatic veins (32), humerus (H), trapezius muscle (Tr), spleen (S).

color, black and white laser prints and transparencies are obtained for lectures and poster presentations and annotated images are preserved on VHS, archived digital tapes, and/or optical disks.

Equipment

Magnetic resonance images are obtained on the 1.5 Tesla GE Signa MR scanner (GE Medical Systems, Milwaukee, Wisconsin). The 3-D reformatted images are videotaped on a separate work console at the monitoring station and computerized color is applied to the images using a ISG console (ISG Technologies Inc, Mississauga, Ontario, Canada). A 512 × 256 matrix format is used.

Case 1

Body Building. The patient is a 37-year-old, 87.0 kilogram asymmetrically built male, with a 6–8 year history of excessive daily body building. He gives a 3 year history of bilateral equal pain in the upper extremities, tingling and numbness of all fingers in the neutral, and stress position (glove-like distribution). He describes an insensitivity to temperature for periods 1–3 days with painful numbness that is improved by weight lifting.

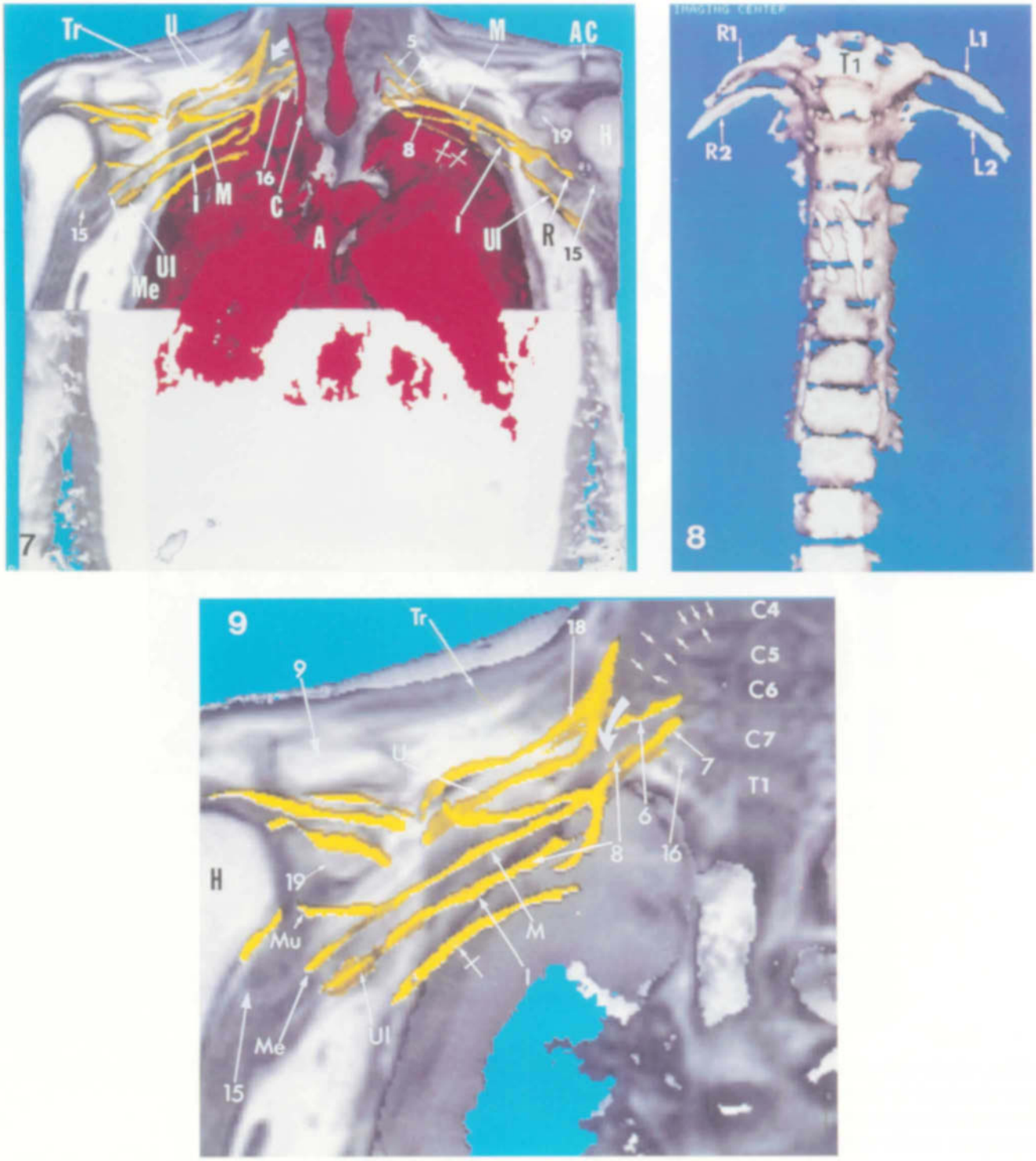

Fig. 7. This is a 3-D reconstructed color image demonstrating the splaying of the right nerve roots (curved white arrow) by an anomalous muscle. Cervical nerve roots (5,6,7), inferior trunk (8), axillary nerve (15), first thoracic nerve (16), coracoid process (19), inferior trunk (I), middle trunk (M), median nerve (ME), ulnar nerve (UL), radial nerve (R), upper trunk (U), trapezius muscle (Tr), humerus (H), right common carotid artery (C), aorta (A), intercostal nerve (bar arrow), acromioclavicular joint (AC).

Nerve conduction studies done at another institution indicate a mild slowing of conduction velocity along the ulnar nerve measured at the elbow and a bilateral borderline increased latency of the median nerve consistent with a carpal tunnel syndrome. Electromyogram (EMG) was normal. Surgery was performed for right carpal tunnel syndrome, but it offered no relief. Urine studies were normal and carcinogenic embryonic antigen (CEA) was borderline on several occasions. Epstein-Barr virus test was positive on multiple occasions following exercise and all other blood studies were negative. He denied taking steroids or alcohol but did take vitamins B, C, and E. A thoracic outlet vascular study and MRI of the cervical spine were performed at another hospital and were negative except for mild degenerative changes at C5–C6 foramina. Referral to our institution revealed minimal deep tendon reflexes, normal Allen's and Tinel's test, and negative Gyon's test and Adson's maneuver. Two point discrimination test was present at 1 cm in the radial, median, and ulnar nerve fields of both hands. The neurological diagnosis was bilateral neurovascular compression of the brachial plexus. An MRI of the brachial plexus was suggested to rule out bilateral compression at the scalene triangle.

The MRI brachial plexus examination demonstrated reduced subcutaneous fat, dilated surface veins, right concave scoliosis of the cervico-thoracic spine, enlarged asymmetric shoulder girdle, and scalene muscles with compression of the neurovascular bundles greater on the right than the left (Figs. 3, 4). Degenerative changes of the acromio-clavicular joint (AC joint) appeared greater on the right and this accentuated the inferior angulation of the clavicle and subclavius muscle which depressed the neurovascular bundle as it exited the scalene triangle. The larger left first fasicle of the serratus anterior muscle seemed to elevate the brachial plexus contributing to the compression of the neurovascular bundle. The scalene triangle compression appeared greater on the right at the junction of the first thoracic nerve root (T1) with the eighth cervical nerve root (Fig. 5a,b). The spinal cord appeared tethered to the right (Fig. 4).

The 3-D color generated images superimposed on the gray scale images confirmed compression of the neurovascular bundles (Fig. 6a–d). The patient was informed of our findings and was advised to stop body building. He requested a second opinion which agreed with our findings of asymmetrical hypertrophic muscular narrowing of the thoracic inlet, accentuated by the secondary degenerative changes of the AC joint with associated cervico-thoracic spine scoliosis.

The patient was advised to stop exercising for 2 weeks, but because he felt better, he resumed exercising and continued to complain of his symptoms.

Case 2

Muscle Anomaly. A 62-year-old male active in sports presented to his private surgeon complaining of numbness, progressive weakness and cramping pain of his right arm. He had loss of grip strength, 12 pounds in the right hand and 50 pounds in the left. He also had difficulty in writing, typing and simple manipulations such as holding a cup. Computerized tomography, MRI of the cervical spine, cerebrospinal fluid, electromyography, and nerve conduction studies done at another institution were reported as normal.

His history was compatible with a right thoracic outlet syndrome. In his physical examination a possible anomalous muscle was detected which the surgeon believed contributed to the diagnosis. The chest radiographs demonstrated right scoliosis of the cervico-thoracic spine, atrophy of the right shoulder girdle muscles, and a low lying right first rib. A diagnosis of right thoracic outlet syndrome was confirmed by the neurological examination.

The MRI sequences confirmed the chest radiographic findings. The coronal sequence demonstrated scoliosis of the cervico-thoracic spine, which was convexed on the right accentuating the elevated transverse process of first thoracic vertebral body. In our studies of the sequential images the right nerve roots were small,

Fig. 8. This is a 3-D reconstructed thoracic spine demonstrating mild scoliosis of thoracic spine. The first thoracic vertebral body (T1) is convexed to the right. The intercostal space is narrower on the side of the convexity and wider on the side of the concavity, right first and 2nd ribs (R1, R2), left first and 2nd ribs (L1, L2).

Fig. 9. This is an enlarged 3-D reconstructed color image of the right brachial plexus in Figure 7 demonstrating proximal displacement of the middle trunk below the inferior trunk. The nerves are straightened as compared to the normal convex course of the left brachial plexus. The 6th cervical nerve root (6) is effaced by the fasicles of the anomalous muscle, 7th cervical nerve root (7), inferior trunk (8), clavicle (9), axillary nerve (15), first thoracic nerve (16), coracoid process (19), inferior trunk (I), middle trunk (M), median nerve (Me), ulnar nerve (UL), upper trunk (U), suprascapular nerve (18), trapezius muscle (Tr), humerus (H), right common carotid artery (C), aorta (A), 2nd intercostal nerve (bar arrow), 5th cervical nerve root (small arrows), cervical vertebral bodies (C4, C5, C6, C7), and first thoracic vertebral body (T1).

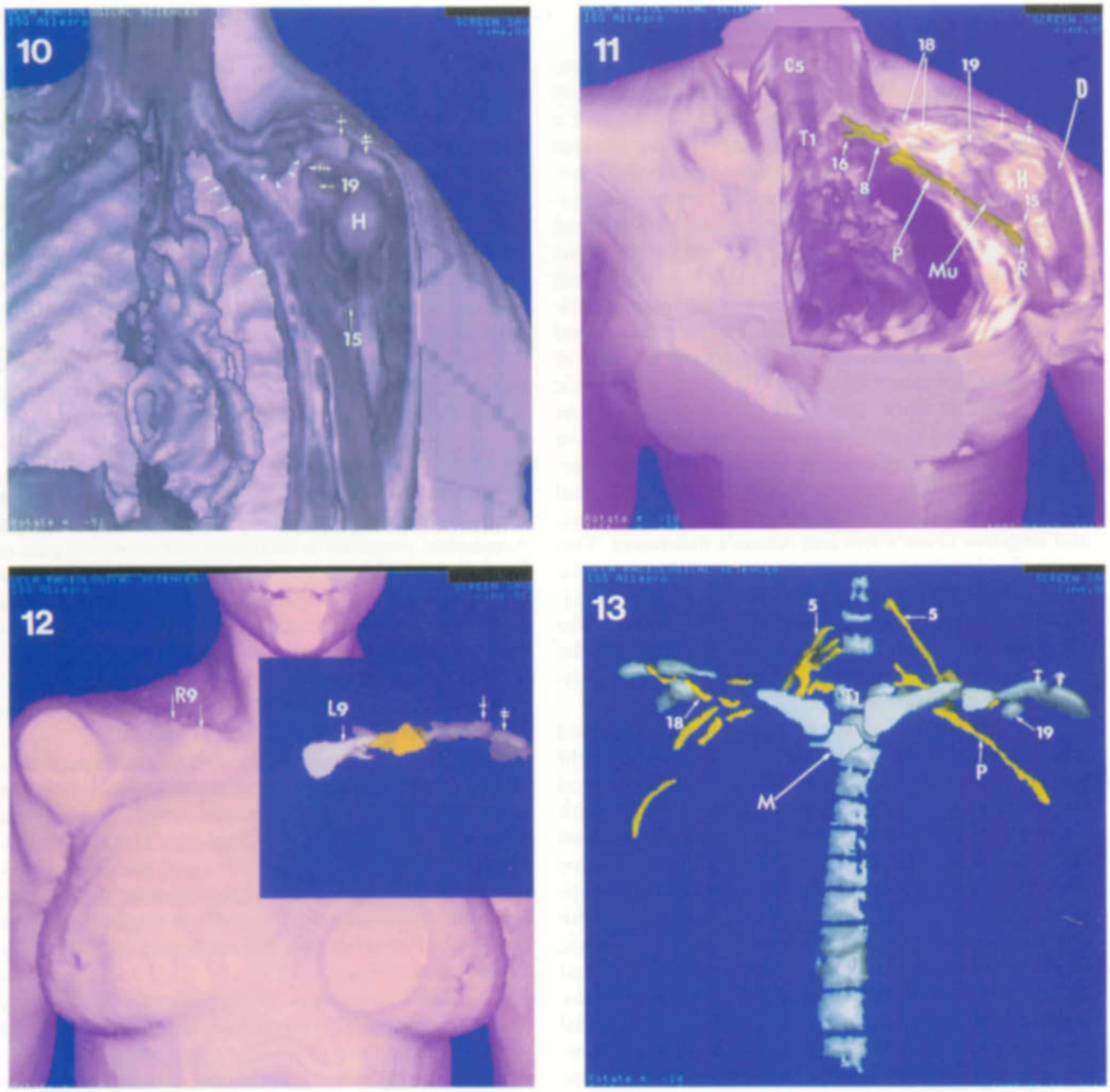

Fig. 10. This is a 3-D reconstructed right posterior oblique image demonstrating the scarred pleura (arrows) and granulation tissue around the fracture (arrowheads). The region of the suprascapular nerve is depressed near the notch of the scapula (3-bar arrow). Axillary nerve (15), coracoid process (19), humerus (H), distal end of the clavicle (Bar arrow), the acromion (2-bar arrow).

Fig. 11. This is a 3-D computer generated image demonstrating the irregular scarring of the inferior trunk (8) and the posterior cord (9). 5th cervical vertebral body (C5), first thoracic vertebral body (T1), first thoracic nerve root (16), axillary nerve (15), suprascapular nerve (18), coracoid process (19), humerus (H), deltoid muscle (D), distal end of the clavicle (bar arrow), the acromion (2-bar arrow).

Fig. 12. This is a 3-D computer generated image demonstrating the remodeled depressed old fracture (yellow) of the left clavicle (L9). The distal clavicle (bar arrow) is elevated and the acromion (2-bar arrow) is depressed. Right clavicle (R9).

Fig. 13. This is a 3-D reconstructed right posterior oblique cervico-thoracic spine demonstrating the secondary changes of fibrosis and scarring to the left nerve roots, posterior cord (P), and trunks (5). The right nerve roots appear curved in this oblique position. Manubrium sternum (M), first thoracic vertebral body (T1), suprascapular nerve (18), coracoid process (19), distal end of the clavicle (bar arrow), the acromion (2-bar arrow).

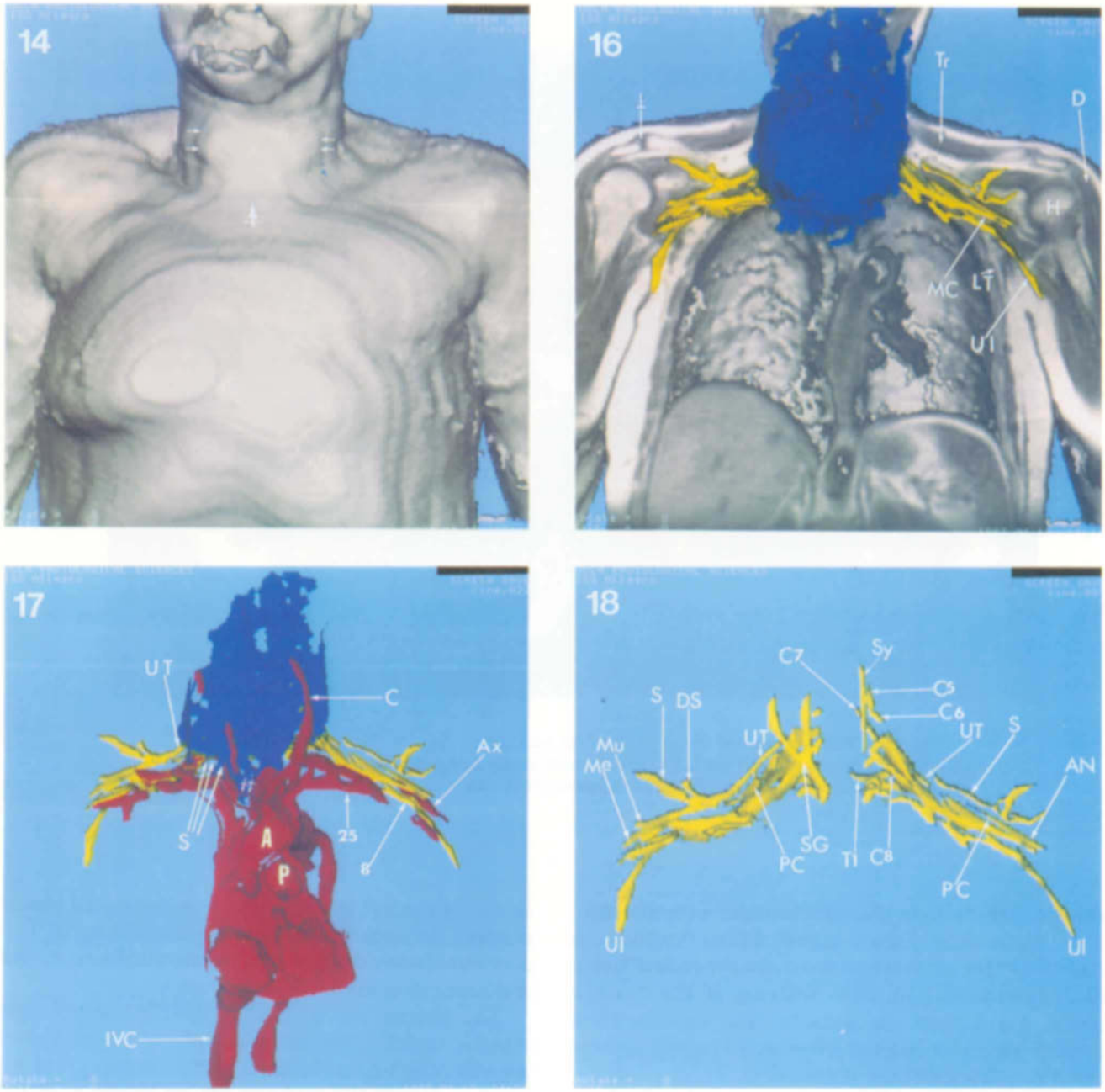

Fig. 14. This is a 3-D computer generated chest image demonstrating the lobulated appearance (small arrows) of the large thyroid mass. The suprasternal notch is obscured (bar arrow).

Fig. 16. This is the 3-D reconstructed coronal chest at the level of the brachial plexus (yellow) demonstrating the thyroid goiter (blue) effacement of the nerves. Acromioclavicular joint (bar arrow), trapezius muscle (Tr), medial cord (MC), long thoracic nerve (LT), ulnar nerve (UL), humerus (H), deltoid muscle (D).

Fig. 17. This is a 3-D reconstructed heart, brachial plexus image demonstrating the effects of the goiter on the great vessels and the nerve roots. The mass displaces the left common carotid artery (C) and left brachial plexus nerve roots as compared to the right. Upper trunk (UT), arch of the right subclavian artery (S), axillary vein (25), ulnar nerve (8), axillary artery (Ax), brachiocephalic artery (bar arrows), aorta (A), pulmonary artery (P), inferior vena cava (IVC).

Fig. 18. This is a 3-D reconstructed image of the brachial plexus demonstrating the compression of the left nerve trunks (at the level of C8) compared to the right nerve trunks. Upper trunk (UT), ulnar nerve (UI), axillary nerve (AN), cervical nerve roots (C5,6,7,8), first thoracic nerve root (T1), suprascapular nerve (S), posterior cord (PC), stellate ganglion (SG), sympathetic plexus (Sy), dorsal scapular nerve (DS), median nerve (Me), musculocutaneus nerve (Mu).

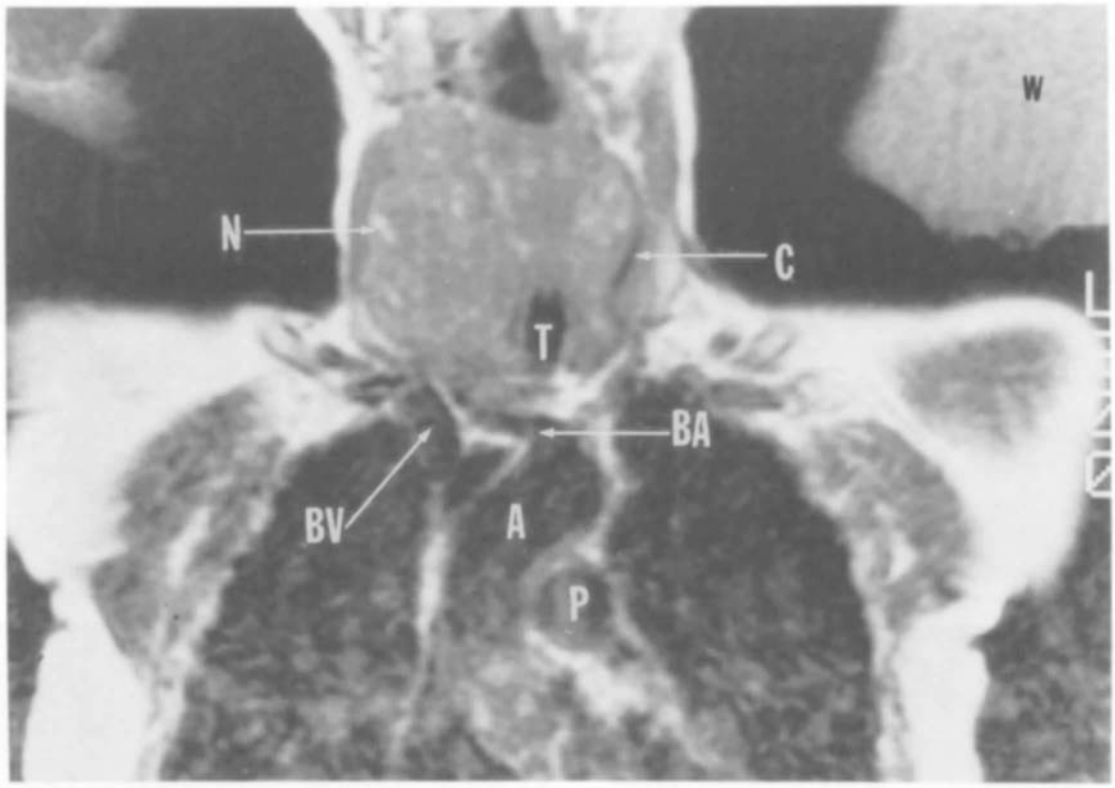

Fig. 15. This is a coronal image of the neck and upper chest at the level of the depressed brachiocephalic artery (BA), aorta (A) and the necrotic thyroid goiter. Brachiocephalic vein (BV), trachea (T), pulmonary artery (P), left common carotid artery (C), necrotic fat (N), saline water bags (W).

straight and the right shoulder muscles were atrophic. The right scalene triangle narrowed from the posterior insertion of the smaller anterior scalene muscle effacing the neurovascular bundle. Splaying of the brachial plexus nerve roots was present. The right coracoid process was lower than the left coracoid process and the vascular structures were patent (Fig. 7).

The transverse, oblique transverse and sagittal images confirmed the above findings. The 3-D reconstruction of the thoracic spine demonstrated slight left angulation of the first thoracic vertebral body (T1) with narrowing of the right first intercostal space (Fig. 8).

In Figure 7, the C5 and C6 nerve roots (curved arrow) appeared splayed by an intermediate gray signal of muscle. The seventh cervical nerve root is shifted both anteriorly and inferiorly at the junction of the eighth cervical nerve and first thoracic nerve (Figs. 7,9). The artery is omitted to demonstrate the upper and middle trunks. The straight appearance of the brachial plexus is accentuated by the narrowed right thoracic cavity. Observe the sharp apex of the right lung compared to the dome shaped left lung apex. The 3-D image (Fig. 7) demonstrates the normal convexed course of the left brachial plexus in the fascial planes crossing the apex of the lung to enter the axilla. The gray scale faintly displays parts of the remaining nerves and other structures.

The patient was advised of our findings of right thoracic outlet syndrome secondary to an anomalous muscle splaying the brachial plexus. Surgery was advised to correct the problem but he sought a second opinion because he believed the problem was secondary to a tumor. The second opinion agreed with our diagnosis.

The right first rib and anomalous muscle were resected. The pain and numbness disappeared and upper arm strength improved, but he continued to have difficulty writing with his right hand.

Case 3

Clavicle Fracture. A 44-year-old lady (49.2 Kg.) suffered severe injuries in an auto accident 20 years ago. She was found unconscious with multiple left rib fractures, left pneumothorax, ruptured spleen, and fractures of the left clavicle and pelvis. She recovered and 10 years later was injured in a second auto accident

when she hyperextended her cervical spine. When lifting heavy boxes, she experienced severe pain in her left upper extremity. The pain radiated over the left shoulder and over the trapezius and pectoral muscles; tingling pain radiated down into the fourth and fifth digits. An MRI of the cervical spine at another hospital demonstrated degenerative disks at C4-C5, C5-C6, and C6-C7 without spinal cord compression. Her clinical evaluation demonstrated hyperirratiblity in the peripheral sensory fields of the ulnar and median nerves. She developed paresthesias in the first, second, fourth, and fifth digits of the left hand and she experienced a loss of hand grip. Muscle atrophy developed in the left shoulder. A diagnosis of left thoracic outlet syndrome was made.

An MRI was requested to evaluate compromise of the left brachial plexus. A review of the chest radiographs demonstrated cervico-thoracic spine scoliosis, a bowed deformity of a low-lying left clavicle and the old fractures of the left upper ribs. Physical examination at the MRI work station confirmed the radiographic and clinical presentation. Gentle pressure over the left clavicle duplicated the complaints of dysesthesias in the left hand.

The coronal MRI confirmed the above clinical findings and demonstrated the low signal intensity of granulation tissue surrounding the old fracture site of the left clavicle. Figure 10 demonstrates the 3-D appearance of the granulation tissue (arrowheads). Observe that the pleural margins are irregular (small arrows) and the irregular border of the brachial plexus gives a shaggy appearance compatible with scarring (Fig. 11). The transverse sequence demonstrated a coracoid process depression of the left brachial plexus. The oblique and sagittal sequences confirmed these findings.

Figure 12 is a partial 3-D color reconstructed image of the lower face, neck, and chest. The left clavicle is irregular shaped, bowed, and angled medially. The old fracture (yellow) is triangular in shape and Figure 11 demonstrates the irregular inferior brachial plexus trunk and the depression of the posterior cord. The inferior trunk follows the scarred pleural margins of the left lung. The low signal intensity of the granulation tissue (Fig. 10, arrowheads) and the fracture site of clavicle are demonstrated in the cut-out (Fig. 12). Observe the concave impression caused by the granulation tissue on the soft tissue structures in the region of the suprascapular nerve in Figure 10. Figure 13 is a right posterior oblique image that demonstrates the 3-D display of the cervico-thoracic spine, clavicles, AC joints, and the coracoid processes. This position accentuates the bowing of the left clavicle and angulation of the left AC joint. The left suprascapular nerve (Fig. 11) is in close apposition to the fracture.

The patient was informed of our findings and surgery was performed to correct the deformity. She has recovered without sequelae.

Case 4

Thyroid Goiter. A 72-year-old woman initially presented with increasing left shoulder edema and pain in the left upper limb. She had a known large thyroid goiter since early childhood. An MRI was ordered to evaluate her left upper limb edema and brachial plexus before possible surgery. Her chest radiographs demonstrated a large irregular lobulated neck mass. The mass extended from the upper limits of her anterior and lateral neck into the ventral part of the superior mediastinum and as far as the middle mediastinum.

The MRI demonstrated an irregular bilateral lobulated large mass displacing normal soft tissue anatomy (Figs. 14–16). The mass contained areas of necrosis and it effaced the venous structures of the neck with depression of the brachiocephalic artery and aorta (Fig. 15). The extension into the soft tissue is demonstrated in Figures 16–18. The esophagus, arteries, veins, and nerves are displaced and the region through which courses the upper part of the left thoracic duct is effaced (Figs. 15, 16.) The greatest compression of the brachial plexus occurs on the left, and this corresponds to the clinical complaints (Figs. 16–18).

Surgery was recommended to debulk the tumor in order to release the vascular and neural compression. Her edema, pain, and syncopal episodes subsided, following removal of the goiter in December 1993.

Case 5

Silicone Breast Implant Rupture. A 53-year-old woman presented in our Breast Clinic with bilateral breast augmentation performed because of postpartum atrophy. The implants ruptured and required replacement. Following replacement, she complained of severe bilateral pain in her breasts and right upper extremity and lumps in the skin over the right chest wall. A right breast biopsy confirmed the migration of silicone material into the fascial planes of the pectoral muscles and axilla. An MRI was requested in order to evaluate her brachial plexopathy and determine the extent of the silicone extravasation.

The T-1 weighted images demonstrated an edematous atrophy of the right shoulder girdle and multiple irregular low intensity signals within the fascial planes of the right pectoralis muscles and brachial plexus. In the right sagittal image of Figure 19, the fascial plane is obscured between the pectoralis major and pectoralis minor muscles. The low signal intensities (SG) are the palpable lumps of silicone granulomas proven at biopsy. The T-1 weighted low signal intensities (SG)

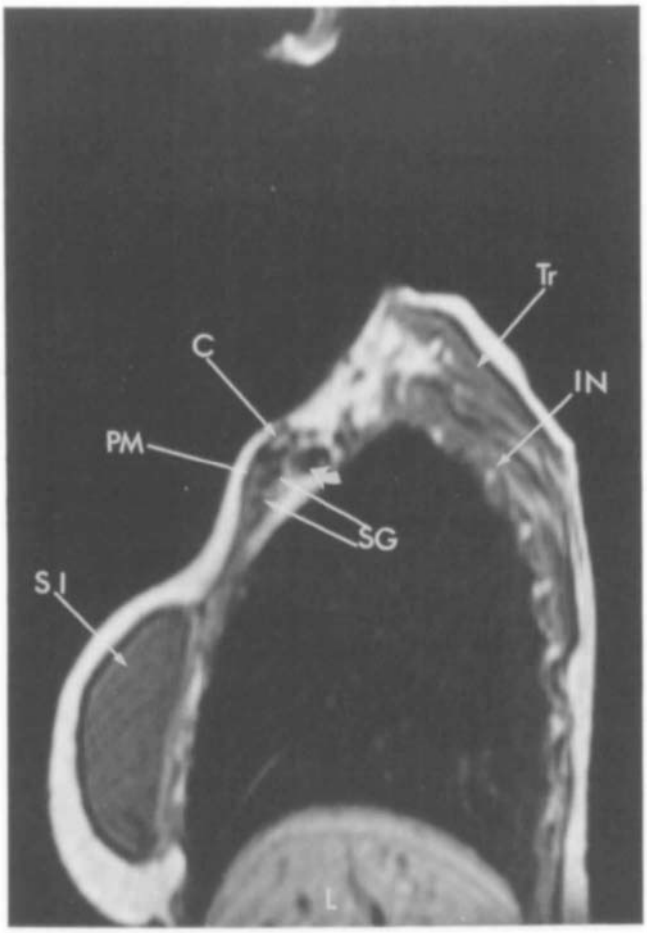

Fig. 19. This is a right sagittal chest image at the level of silicone breast implant rupture (SG) infiltrating the pectoralis major muscle. Pectoralis major muscle (PM), clavicle (C), silicone implant (SI), trapezius muscle (Tr), intercostal nerve (IN). Silicone granuloma overlying the vascular structures in the axilla (curved white arrow).

were confirmed as high signal intensities on the T-2 weighted series.

The site of rupture was identified as a sharp peak (tear drop sign) of the silicone implant (red color; curve solid white arrow, Fig. 20). The gray scale coronal images demonstrated a possible rupture along the medial aspect of the implant. Figure 20 demonstrates the possible site of impending rupture (a large bulge, small arrows) and the extruded silicone (curved transparent arrow) overlying the brachial plexus inferior to the coracoid process (CP).

The patient was informed of our findings and underwent surgery to remove the ruptured implant and the extruded silicone from the chest wall and neck. A follow-up MRI examination in February 1994 demonstrated residual fibrosis between the right pectoral muscles and fibrotic changes of the brachial plexus cords lateral to the scalene triangle. No silicone-like granulomas were detected, but the patient still has complaints of pain and weakness of the right arm and hand.

DISCUSSION

Knowledge of landmark anatomy and knowledge of the blood supply of the normal brachial plexus correlated with the clinical history are necessary for understanding compromising brachial plexopathies displayed by MRI. The images are not obtained in the same anatomical position displayed in most textbooks. The required scanning position often results in an aggravation of the presenting clinical complaints. This is due to scapular pressure upon the brachial plexus because of the supine confinement necessary during the imaging sequence.

The problem in Case 1 (**bodybuilder**) is caused by several sites of compression upon the brachial plexus: 1) scalene triangle compression by the scalene muscles as the neurovascular bundle is formed, 2) the sternocleidomastoid muscle, and 3) the clavicle and subclavius muscle at the thoracic outlet. The cervicothoracic scoliosis may be secondary to the shorter insertion of the anterior scalene muscle on the first rib, and/or the asymmetric muscular development of the shoulder girdle muscles (Figs. 3, 4). Surgery in this case may be complicated by problems caused by the hypertrophy of the muscles.

In Case 2, the **anomalous muscle** interdigitated and splayed the nerve roots before their entrance into the scalene triangle causing interscalene compression of the inferior trunk of the brachial plexus. Although this anomaly has been well described in the literature (Sunderland, 1968; Lord, 1971), it has not been reported using MRI. Lord (1971) considered cases such as this to be congenital with aging and musculoskeletal laxity playing a definitive role. Surgery is often performed and the compression is relieved; however Sunderland (1968) states that the time factor may play an important role in a patient's recovery. In cases of long term compression, the effects of disuse atrophy and ischemia persisted.

Cases of **clavicular fracture** (Case 3) are in a special category, where secondary changes of fibrosis and scarring compromise the brachial plexus. The clavicle is normally arched and curved, allowing passage of the neurovascular bundle into the axilla. In this case, the fractured ends of the clavicle overlap, shortening the bone length. This alters the architecture of the bone and fascial planes resulting in neurovascular compro-

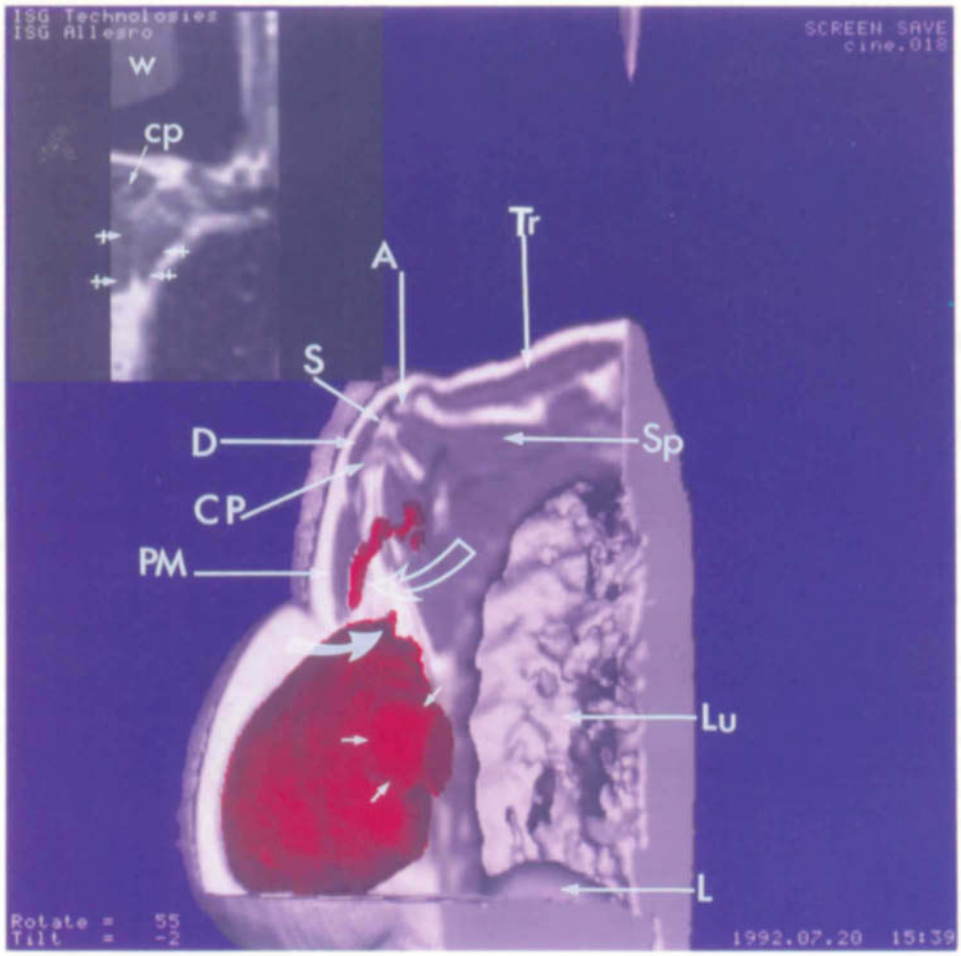

Fig. 20. The is a 3-D color reconstructed coronal image cut away to demonstrate the rupture site of the silicone implant and the silicone infiltrating the brachial plexus at the coracoid process. The acromion (A), deltoid muscle (D), suprascapular nerve on end (S), trapezius muscle (Tr), coracoid process (CP), supraspinatus muscle (Sp), lung (Lu), liver (L), site (curved white arrow), silicone crossing the nerves (curved clear arrow), impending rupture site (small arrows). The gray scale image is at the upper left corner, water bag (W), low signal intensities of the silicone granulomas (bar arrows).

mise. The granulation tissue narrows the tunnel for the brachial plexus and ischemia develops. This compounds the fibrosis which resulted from the traumatic injury. The patient's age, disuse atrophy, and musculoskeletal laxity compounds the compromise (Lord and Rosati, 1971). The strain when heavy boxes were lifted embarrassed the neurovascular structures causing the clinical complaints. Following surgery, pressure was relieved and the patient remains symptom free.

To our knowledge the mass effect of a **thyroid goiter** (Case 4) displayed by MRI compressing brachial plexus roots and trunks and the great vessels has not been described in the literature as a cause of brachial plexopathy. In the radiological literature, thyroid masses may be observed as anterior mediastinal densities. We believe that large thyroid goiters should be considered as a possible cause of brachial plexopathy, particularly when they extend beyond the subclavian vessels.

Silicone-breast implant ruptures (Case 5) may demonstrate the pressure effects of mass-like lesions on subcutaneous tissues and on the brachial plexus. In these patients the brachial plexus maybe compressed at the coracoid process, the supraclavicular fossa or within the scalene triangle. Following surgical removal of the extravasated silicone and the ruptured capsule, lymphatic drainage is altered and may result in metaplasia and edema which contribute to the pressure effects on the neurovascular bundle (Collins et al., 1991a).

We are aware that other conditions such as protruding cervical discs, somatic dysfunction of the thoracic nerve roots (sympathetics), arthritis, and tumors may

also cause pain and paresthesias. Diagnosis of compression of the brachial plexus, such as reported in our cases, must be distinguished from these other lesions that may also produce pain and paraesthesia in the shoulder, arm, and hand. A tailored anatomic imaging approach to the evaluation of the brachial plexus using MRI allows us to distinguish among the various etiologies of the clinical complaints.

ACKNOWLEDGMENTS

The authors thank Dr. Carmine D. Clemente for reviewing the manuscript.

REFERENCES

Clemente, C. D. 1985 Gray's Anatomy. 31st American Edition. Philadelphia. Lea and Febiger.

Clemente, C. D. 1987 Anatomy, A Regional Atlas of The Human Body. 3rd Ed, Baltimore: Urban and Schwarzenberg.

Collins, J. D., P. Batra, K. Brown, and M. L. Shaver 1986 Anatomy of the thorax and shoulder girdle as displayed by magnetic resonance imaging. Anat. Rec., *214*:24A.

Collins, J. D., M. L. Shaver, P. Batra, and K. Brown 1989a Nerves on magnetic resonance imaging. J. Natl. Med. Assoc., *81*:129–134.

Collins, J. D., P. Batra, K. Brown, and M. L. Shaver 1989b Anatomy of the thorax and shoulder girdle displayed by magnetic resonance imaging. J. Natl. Med. Assoc., *83*:26–32.

Collins, J. D., P. Batra, K. Brown, and M. L. Shaver 1991a Magnetic resonance imaging of chest wall lesions. J. Natl. Med. Assoc., *83*:352–360.

Collins, J. D., M. L. Shaver, A. C. Disher, P. Batra, K. Brown, and T. Q. Miller, 1991b Imaging the thoracic lymphatics: Experimental studies of swine. Clin. Anat. *4*:433–446.

Collins, J. D., A. Disher, T. Q. Miller, and M. L. Shaver, 1993 Compromising abnormalities of the brachial plexus as displayed by magnetic resonance imaging. Anat. Rec. *1*:44A.

Dyck, P. K., J. Karnes, H. Lais, E. P. Lofgren, and J. C. Stevens 1984 Pathological alterations of the peripheral nervous system of humans: Peripheral Neuropathy. 2nd ED. Philadelphia: W. B. Saunders, pp. 760–870.

Lord, J. W., L. M. Rosati 1971 Thoracic-outlet syndromes. Clinical Symposia-Geigy, *23*:1–32.

Lord, J. W., 1989 Critical reappraisal of diagnostic and therapeutic modalities for thoracic outlet syndromes. Surgery, Gynecol Obstet 168:337–340.

Sunderland, S., 1945 Blood supply of the nerves to the upper limb in man. Arch Neurol Psych., *53*:91–115.

Sunderland, S., 1968 Nerves and Nerve Injuries, Baltimore. Williams & Wilkins Co.